

## Electronic Supplementary Information

### **Metallic MoS<sub>2</sub> Nanosheets: Multifunctional Electrocatalysts for ORR, OER and Li-O<sub>2</sub> Batteries**

Zoya Sadighi,<sup>a</sup> Jiapeng Liu,<sup>a</sup> Ling Zhao,<sup>a</sup> Francesco Ciucci<sup>ab</sup> and Jang-Kyo Kim<sup>\*a</sup>

<sup>a</sup> *Department of Mechanical and Aerospace Engineering, The Hong Kong University of Science  
and Technology, Clear Water Bay, Hong Kong*

<sup>b</sup> *Department of Chemical and Biomolecular Engineering, The Hong Kong University of Science  
and Technology, Clear Water Bay, Hong Kong*

\*Corresponding author. J.-K. Kim. E-mail: mejkkim@ust.hk. Tel: +852 2358 7207, Fax: +852  
2358 1543.

## Supplementary note 1: Preparation of electrode materials

*Exfoliation of bulk MoS<sub>2</sub> to form 1T-MoS<sub>2</sub> nanosheets.* Two dimensional (2D) 1T-MoS<sub>2</sub> was prepared *via* liquid-redox intercalation and exfoliation of bulk MoS<sub>2</sub> precursor. Typically, 0.1 g MoS<sub>2</sub> (Sigma-Aldrich, 99%) was dispersed in 20 mL N-Methyl-2-pyrrolidone (NMP, Sigma-Aldrich, 99%) under probe sonication for 30 min at 400 W power. An antioxidant solution was prepared by dissolving 0.4 g sodium borohydride (NaBH<sub>4</sub>, Sigma-Aldrich, 99%) and 0.2 g sodium hydroxide (NaOH, BDH, 99%) in 15 mL methanol. Immediately after preparing the antioxidant solution, it was dropwisely added to MoS<sub>2</sub> in NMP mixture under probe sonication. Due to the highly exothermic reaction of antioxidant reagent with the MoS<sub>2</sub> precursor, the sonication was carried out in an ice bath using an alternative on/off routine of 7 sec on and 3 sec off to prevent overheating. The sodium intercalated MoS<sub>2</sub> powder in metallic phase, 1T-Na<sub>x</sub>MoS<sub>2</sub>, was obtained after vacuum infiltration. 100 mg 1T-Na<sub>x</sub>MoS<sub>2</sub> powder was dispersed in 15 mL dimethylformamide (DMF, Sigma-Aldrich, 99%) using probe sonication for 1 h at 400 W power as in the above experiment. Exfoliated 1T-Na<sub>x</sub>MoS<sub>2</sub> nanosheets (NSs) were collected after centrifugation at 12,000 rpm for 30 min, and diluted in deionized (DI) water to remove the sodium cations of NaOH (1T-Na<sub>x</sub>MoS<sub>2</sub> + H<sub>2</sub>O → 1T-MoS<sub>2</sub> + NaOH + H<sub>2</sub> (g)),<sup>S1-S3</sup> which are designated as 1T-MoS<sub>2</sub>. The 1T-MoS<sub>2</sub> NSs were redispersed in DMF at a concentration of 10 mg ml<sup>-1</sup> for long-term storage because of their high stability in DMF.<sup>S4</sup>

*Preparation of oxygen electrodes.* Multi-walled carbon nanotubes (MWCNTs, average diameter of 50 nm and 10 μm in length, supplied by Shenzhen Nanotech) were purified in nitric acid at room temperature for 12 h to remove any metallic impurities and functionalize their surface.<sup>S5</sup> The purity of functionalized CNTs after acid treatment is shown using the XRD and XPS analyses (Fig. S1). The XRD spectrum (Fig. S1a) revealed three peaks at ~26.2, 44.4 and 54° corresponding to

the (002), (101) and (004) planes, respectively. The XPS spectrum (Fig. S1b) represent C 1s, N 1s and O 1s peaks resulting from acid functionalization. 10 mg of functionalized CNTs were dispersed in 20 mL DMF under probe sonication for 30 min at 400 W. 7 ml of 10 mg ml<sup>-1</sup> 1T-MoS<sub>2</sub> in DMF was mixed with 6 ml of the above mixture under bath sonication until a homogeneous mixture was achieved. The product was redispersed in DI water and 1T-MoS<sub>2</sub>/CNT papers (1T-MoS<sub>2</sub>: CNT wt. ratio = 7:3) were obtained using vacuum infiltration of the dispersion followed by drying in a vacuum oven at 60 °C for 12 h. Freestanding and binder-free oxygen electrodes were prepared by cutting the paper into square pieces of ~1 mg in weight and 1.2 cm in side. Electrodes were also made from the 2H-MoS<sub>2</sub>/CNT papers prepared from the bulk MoS<sub>2</sub> crystals and functionalized CNTs by dispersing them in DI water under the same condition as above and vacuum infiltration of the dispersion.

### **Supplementary note 2: Characterization**

Si/SiO<sub>2</sub> wafers cleaned with Piranha solution, H<sub>2</sub>SO<sub>4</sub>:H<sub>2</sub>O<sub>2</sub> = 7:3, were immersed into the exfoliated 1T-MoS<sub>2</sub>/ethanol dispersion to collect the NSs. The thickness of NSs was measured by atomic force spectroscopy (AFM, NanoScope IIIa/Dimension 3100) with Laser radiation of 1.0 mW Max at 670 nm. The NSs after infiltration were observed by field emission scanning electron microscopy (FESEM, JEOL-6700F). The structure of 1T-MoS<sub>2</sub>/CNT oxygen electrode was examined by FESEM (JEOL-7100F) and transmission electron microscopy (TEM, JEOL 2010). The high resolution TEM (HRTEM) was applied to observe the atomic arrangements. Their elemental maps were obtained by energy dispersive X-ray spectroscopy (EDX) on the FESEM images. The crystallinity of different MoS<sub>2</sub> phases were studied by X-ray diffraction (XRD, Philips PW1830) analysis with Cu K $\alpha$  radiation at room temperature and 2 $\theta$  = 10-80°. Raman spectroscopy (RS, Renishaw PLC) was conducted at a laser excitation wavelength of 514 nm. The

surface chemistries were analyzed by performing the X-ray photoelectron spectroscopy (XPS, PHI5600, Physical Electronics) using Al K $\alpha$  X-ray spectrometer at 14 kV and the spectra were calibrated with C 1s (285 eV). Thermal gravimetric (TG) and differential scanning calorimetry (DSC) analyses were conducted in an O<sub>2</sub> atmosphere over a temperature range of 20-200 °C at a heating rate of 10 °C min<sup>-1</sup>. A four-probe resistivity/Hall system (HK5500PC, Bio-Rad) was used to measure the electrical conductivities.

### **Supplementary note 3: Electrochemical measurements**

*Lithium-oxygen battery (LOB).* LOBs were tested using a custom-built device as in our previous studies.<sup>S5,S6</sup> The 1T-MoS<sub>2</sub>/CNT or 2H-MoS<sub>2</sub>/CNT cathode, lithium foil, glass fiber separator (Whatman, GF/D), 0.5 LiTFSI in TEGDME solution as electrolyte were used to construct the LOB cell. The carbon papers (TGP-H-060 supplied by Toray Co.) of 0.19 mm in thickness were cut into disks of 14 mm in diameter as the gas diffusion layer and current collector. The weight of freestanding materials, ~1 mg, was applied to calculate the specific capacities and current densities. The LOB cells were purged with pure O<sub>2</sub> (>99.9992%) for 0.5 h before the electrochemical tests. To reach a stable open-circuit voltage, the cells were left idle for 3 h before start discharging. A LAND 2001 CT battery tester was used to determine the discharge/charge curves in the potential range of 2.0-4.5 V. The cyclic tests were conducted at a current density of 200 mA g<sup>-1</sup> and an upper-limit capacity of 500 mAh g<sup>-1</sup>. The electrochemical impedance spectroscopy (EIS) analysis was performed at different stages of discharge/charge process in the frequency range between 10 mHz and 100 kHz and at a constant perturbation amplitude of 5 mV on a CHI660c electrochemical workstation. The cyclic voltammetry (CV) tests were conducted at scan rates varying from 0.1 to 0.3 mV s<sup>-1</sup> in the potential range of 2-4.5 V.

*Oxygen reduction/evolution reactions (ORR/OER).* The ORR and OER catalytic activities of various electrode materials, including 2H-, 1T-MoS<sub>2</sub>, edge-oxidized 1T-MoS<sub>2</sub>, 2H-MoS<sub>2</sub>/CNT and Pt/C were investigated using a standard three-electrode system with rotating ring disc electrode apparatus (RRDE-3A, BAS Inc.) and a potentiostat (ALS2325E, BAS Inc.) in an O<sub>2</sub> saturated 0.1 M KOH electrolyte. A mixture of 4 mg catalyst, 980 μL ethanol and 20 μL Nafion solution was ultrasonicated for 30 min to prepare catalyst ink, which was used as the working electrode by applying on the Pt-glassy carbon electrode of 0.1255 cm<sup>2</sup> in area with a catalyst loading of 0.32 mg cm<sup>-2</sup>. Pt and Ag/AgCl were used as the counter and the reference electrodes, respectively. The ORR activity was measured using linear scanning voltammetry (LSV) at a potential window ranging from 0 to -0.8 V (vs Ag/AgCl) at different rotation speeds of 400, 900, 1600 and 2500 rpm. The transferred electron number (n) was determined from the slop of Koutecky-Levich (K-L) lines,  $j^{-1}$  versus  $\omega^{-1/2}$ , based on the K-L Equations S1 and S2. The K-L plots (Fig. 5d) were obtained at different potentials and different rotational speeds in the LSV curves.

$$\frac{1}{j} = \frac{1}{j_L} + \frac{1}{j_K} = \frac{1}{B} \omega^{-1/2} + \frac{1}{j_K} \quad (\text{S1})$$

$$B = 0.62D^{2/3}v^{-1/6}nFC \quad (\text{S2})$$

where  $j$ ,  $j_L$  and  $j_K$  are the measured, mass-transport-limited and kinetic-limited current densities, respectively. At a certain potential,  $j_K$  is assumed to be constant.  $j_L$  is proportional to the square root of electrode rotational speed ( $\omega$ ).  $D = 1.9 \times 10^{-5}$  cm<sup>2</sup> s<sup>-1</sup> is the diffusion coefficient of O<sub>2</sub> in 0.1 M KOH,  $v = 0.01$  cm<sup>2</sup> s<sup>-1</sup> is the kinematic viscosity of the electrolyte,  $F = 96,485$  C mol<sup>-1</sup> is the Faraday constant and  $C = 1.2 \times 10^{-6}$  mol cm<sup>-3</sup> is the bulk concentration of O<sub>2</sub>.<sup>S8</sup>

The OER activity was tested from 0 to 0.8 V (*vs* Ag/AgCl) at 1600 rpm. Both ORR and OER tests were executed at a scan rate of 5 mV s<sup>-1</sup>. The measured potentials were converted to the reversible hydrogen electrode (RHE) using Equation S3:

$$E_{\text{RHE}} = E_{\text{Ag/AgCl}} + 0.059\text{pH} + E^{\circ}_{\text{Ag/AgCl}} \quad (\text{S3})$$

where  $E_{\text{RHE}}$  is the potential against RHE,  $E_{\text{Ag/AgCl}}$  is the experimentally measured potential against Ag/AgCl, and  $E^{\circ}_{\text{Ag/AgCl}}$  is the standard potential at 25 °C (0.1976 V).<sup>S9</sup>

*Electrochemically active surface area (ECSA) calculations.* The ECSA was calculated according to Equation S4:

$$\text{ECSA} = C_{\text{dl}}/C_{\text{s}} \quad (\text{S4})$$

where  $C_{\text{dl}}$  is the measured double layer capacitance of samples (in mF) with a surface area of considering the surface area of 0.1255 cm<sup>2</sup>,  $C_{\text{s}}$  is the specific capacitance of the catalyst ( $C_{\text{s}} = 0.04$  mF cm<sup>-2</sup> in 0.1 M KOH).  $C_{\text{dl}}$  was calculated using CVs in the potential range of 0.91-1.11 V (*vs* RHE) at various scan rates (40-180 mV s<sup>-1</sup>). The difference in current density ( $\Delta J = J_{\text{a}} - J_{\text{c}}$ ) at 1.0 V (*vs* RHE) was plotted against scan rates and the  $C_{\text{dl}}$  was obtained from the slope (Fig. 6).<sup>S9,S10</sup>

#### **Supplementary note 4: DFT calculations**

The DFT calculations were carried out following our recent studies.<sup>S10,S11</sup> All the spin-polarized first-principle calculations were performed using the Vienna *ab initio* simulation package<sup>S14</sup> with a plane wave basis set and a projector-augmented wave approach.<sup>S15</sup> The kinetic energy cutoff was set at 500 eV and the exchange-correlation was described using the Perdew-Burk-Ernzerhof functional<sup>S16</sup> under the generalized gradient approximation scheme. For both 2H and 1T phases, 4×4 monolayer MoS<sub>2</sub> was used in which 16 Mo atoms and 32 S atoms were included. The *van der*

*Waals* correction was implemented in the D3 scheme.<sup>S17</sup> These atoms were allowed to relax using the conjugated gradient method until a convergence criterion of  $10^{-5}$  eV for energy and 0.02 eV/Å for force.

The optimized lattice constants of the 2H-MoS<sub>2</sub> and 1T-MoS<sub>2</sub> phases were 3.162 and 3.177 Å, respectively, which agreed with the previously reported values.<sup>S18</sup> To simulate the adsorption of Li atom, O<sub>2</sub> and Li<sub>x</sub>O<sub>y</sub> molecules on the MoS<sub>2</sub> surface, its basal planes were constructed with a 15 Å vacuum space along the *c*-direction to cancel the interactions between different slabs. The adsorption of O<sub>2</sub> on the edges were simulated using the edge model of another 15 Å vacuum space along the *b* direction. The Brillouin-zone was sampled by Gamma centered k-meshes of 4×4×1 and 4×1×1 for the basal plane and edge models, respectively. The adsorption energies of different initial species (Li or O<sub>2</sub>) were calculated using Equation S5:

$$E_{(O_2/Li)_{ads}} = E_{MoS_2+(O_2/Li)} - E_{MoS_2} - E_{O_2/Li} \quad (S5)$$

where  $E_{MoS_2+(O_2/Li)}$  is the energy of monolayer MoS<sub>2</sub> with adsorbed O<sub>2</sub> molecules or Li atoms on it,  $E_{MoS_2}$  is the energy of pristine MoS<sub>2</sub> monolayer, and  $E_{O_2/Li}$  corresponds to the energy of Li in bulk metal state or O<sub>2</sub> molecule in a triple state to eliminate the over-binding problem.

To characterize the adsorption reaction of discharge products, Li<sub>x</sub>O<sub>y</sub> (Li<sub>2</sub>O<sub>2</sub> or LiO<sub>2</sub>), on the surface, the adsorption energy is defined as follows:

$$E_{(Li_xO_y)_{ads}} = E_{MoS_2+Li_xO_y} - E_{MoS_2} - nE_{Li} - E_{O_2} \quad (S6)$$

where  $E_{MoS_2+Li_xO_y}$  is the total energy of Li<sub>2</sub>O<sub>2</sub> or LiO<sub>2</sub> adsorbed on the surface of MoS<sub>2</sub>, and *n* is the number of Li atoms in Li<sub>2</sub>O<sub>2</sub> or LiO<sub>2</sub>, either 2 or 1. Finally, for the formation of Li<sub>2</sub>O<sub>2</sub> during ORR, different steps of reaction free energies were calculated using Equation S7:

$$\Delta G_n = E_{tot(n)} - E_{tot(n-1)} - E_{ori} \quad (S7)$$

where  $E_{tot(n)}$ ,  $E_{tot(n-1)}$  and  $E_{ori}$  represent the total binding energies of the adsorption configuration at the (n)<sup>th</sup> step, at the (n-1)<sup>th</sup> step, and the original energy of the adsorbed species (Li or O<sub>2</sub>).<sup>S19</sup>

### Supplementary note 5: Lithium diffusion coefficients calculations

The kinetics of oxygen electrochemical process in the LOB cell was studied using the CV curves. Due to the electro-activation process of oxygen electrode in the first cycle, the CV curves in the third and following cycles were measured at different rates (Figs. S2d, e). The oxidation peak currents,  $I_p$ , indicated by the arrows are plotted versus the square root of scan rate,  $v^{1/2}$ , in Fig. S2f. The linear relationship between  $I_p$  and  $v^{1/2}$  suggests a diffusion-controlled reaction, where the Randles-Sevick relationship given by Equation S8 is applicable:<sup>S20</sup>

$$I_p = 0.4463 nFAC(nFvD/RT)^{1/2} = [269,000 n^{3/2}AD^{1/2}C]v^{1/2} \quad (S8)$$

where  $269,000 n^{3/2}AD^{1/2}C = B$ , which can be directly taken from the slope of the linear relationship between  $I_p$  and  $v^{1/2}$  (Fig. S5f).

### Supplementary note 6: Warburg factor calculations

The real impedance ( $Z'$ ) data at a low frequency range are plotted as a function of minus square route of frequencies (Fig. S2a). The Warburg factor ( $\sigma$ ), the only variable parameter in Equation S9, was calculated directly from the slope of the linear relationship:

$$D_{Li} = \frac{R^2 T^2}{2A^2 n^4 F^4 C^2 \sigma^2} \quad (S9)$$

where  $R$  is the gas constant;  $T$  the temperature;  $A$  the electrode area ( $= 1.4 \text{ cm}^2$ );  $n$  the number of electrons transferred in the redox reactions ( $= 2$ );  $F$  the Faraday constant; and  $C$  the concentration

of lithium ions ( $= 0.001 \text{ mole cm}^{-3}$ ).<sup>S21</sup> This method was repeated to the EIS spectra of both the 1T-MoS<sub>2</sub>/CNT and 2H-MoS<sub>2</sub>/CNT electrodes during different stages of cycles (Fig. S5b, c) to acquire the Warburg factors (Fig. 3i).

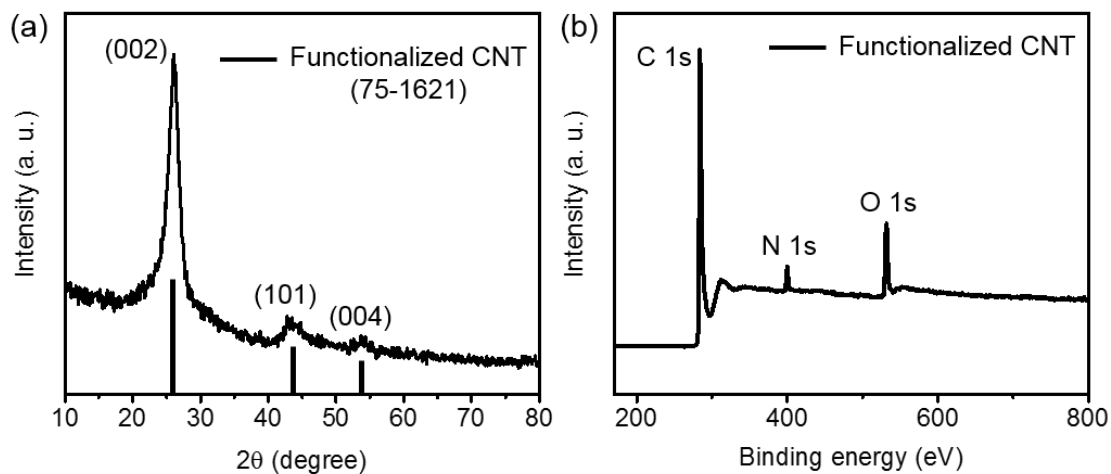


**Figure S1.** XRD (a) and XPS (b) spectra of functionalized CNTs.

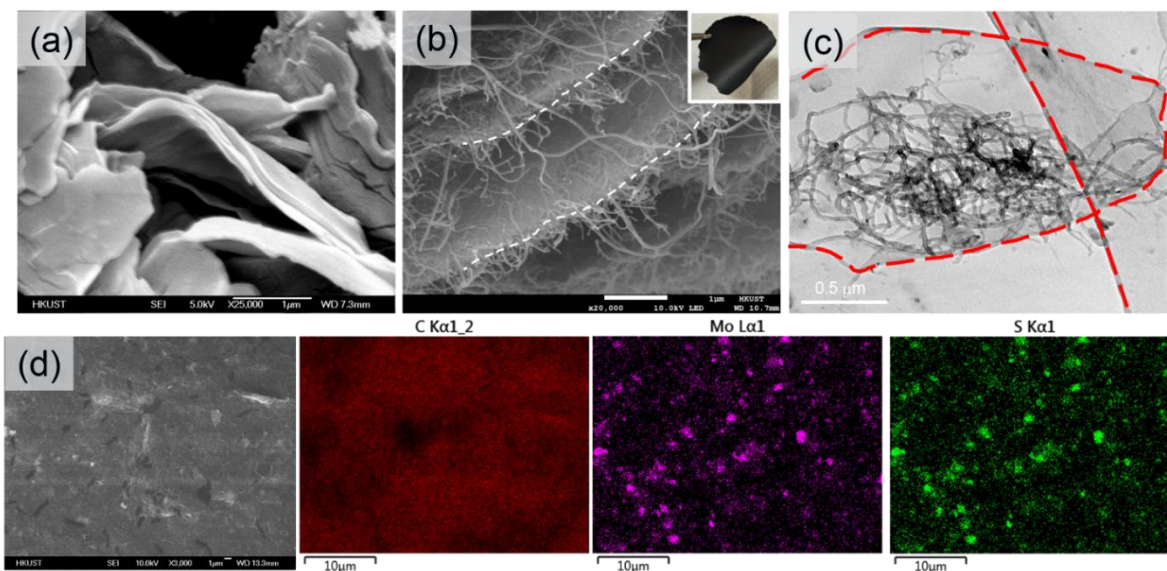


**Figure S2.** SEM images of (a) 1T-MoS<sub>2</sub> and (b) 1T-MoS<sub>2</sub>/CNT. White dotted lines indicate 2D sheets in (b). Inset in (b) shows the freestanding 1T-MoS<sub>2</sub>/CNT paper. (c) TEM image for 1T-

MoS<sub>2</sub>/CNT. 1T-MoS<sub>2</sub> NSs are designated with red dashed lines. (d) EDX elemental maps related to SEM image for 1T-MoS<sub>2</sub>/CNT.

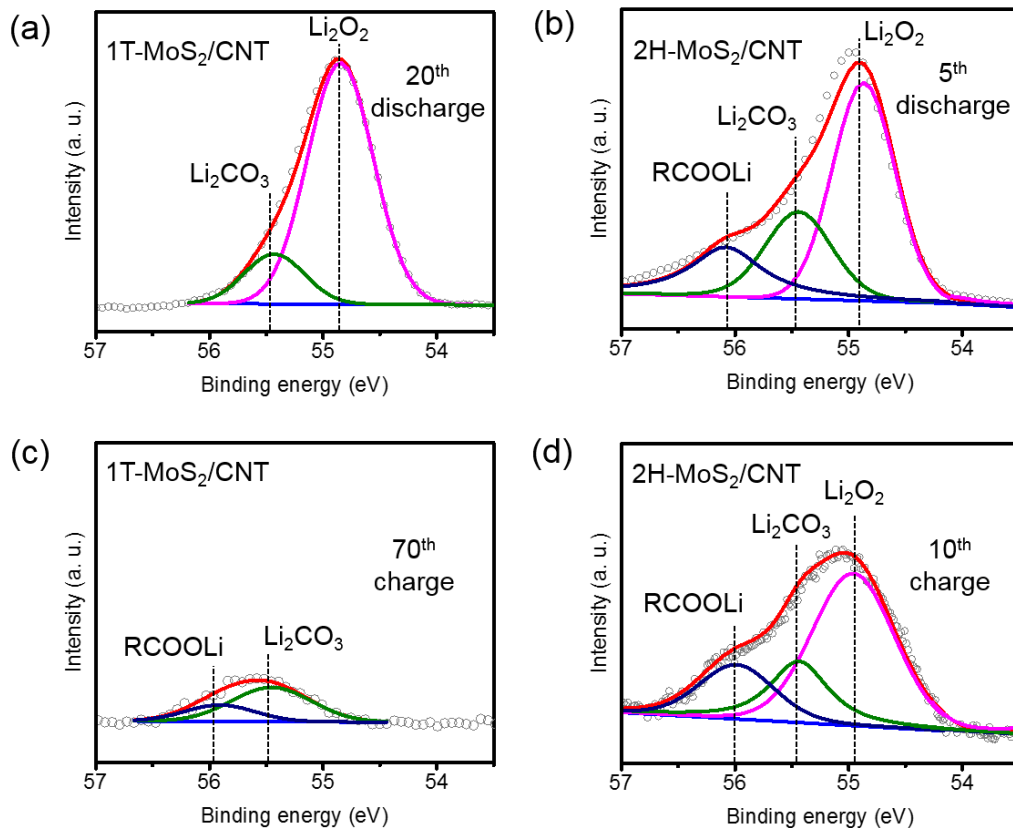


**Figure S3.** *Ex situ* XPS spectra: deconvoluted Li 1s of the (a and c) 1T-MoS<sub>2</sub>/CNT and (b and d) 2H-MoS<sub>2</sub>/CNT electrodes at different discharge and charge stages.

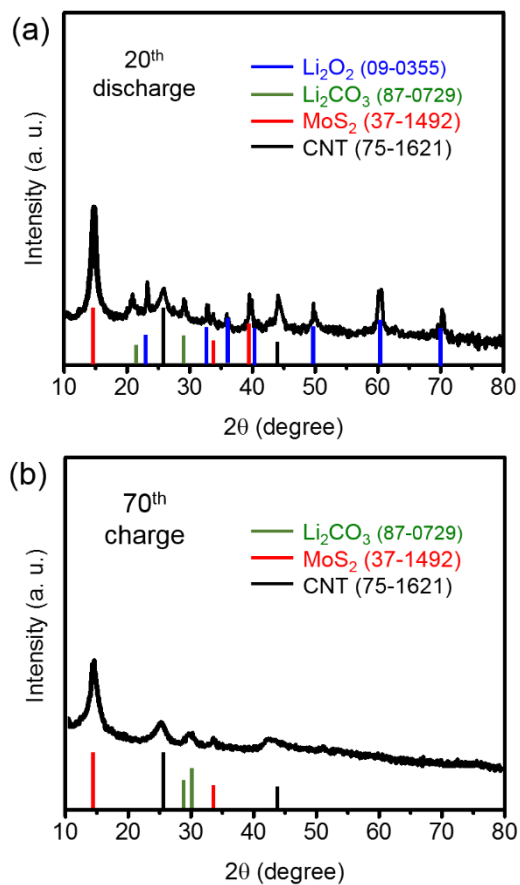


**Figure S4.** *Ex situ* XRD spectra of the 1T-MoS<sub>2</sub>/CNT electrode taken after (a) the 20<sup>th</sup> discharge and (b) the 70<sup>th</sup> charge at 200 mA g<sup>-1</sup> at an upper-limit capacity of 500 mAh g<sup>-1</sup>.

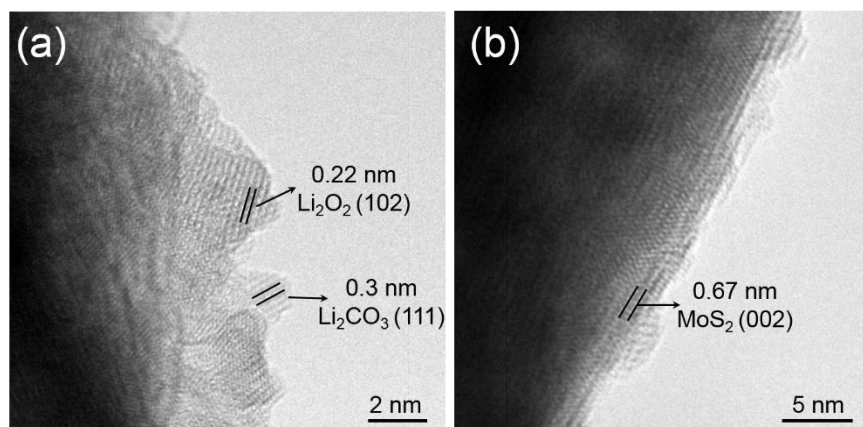


**Figure S5.** HRTEM images of 1T-MoS<sub>2</sub> after (a) the formation of Li<sub>2</sub>O<sub>2</sub> upon discharge and (b) the decomposition of Li<sub>2</sub>O<sub>2</sub> upon charge.

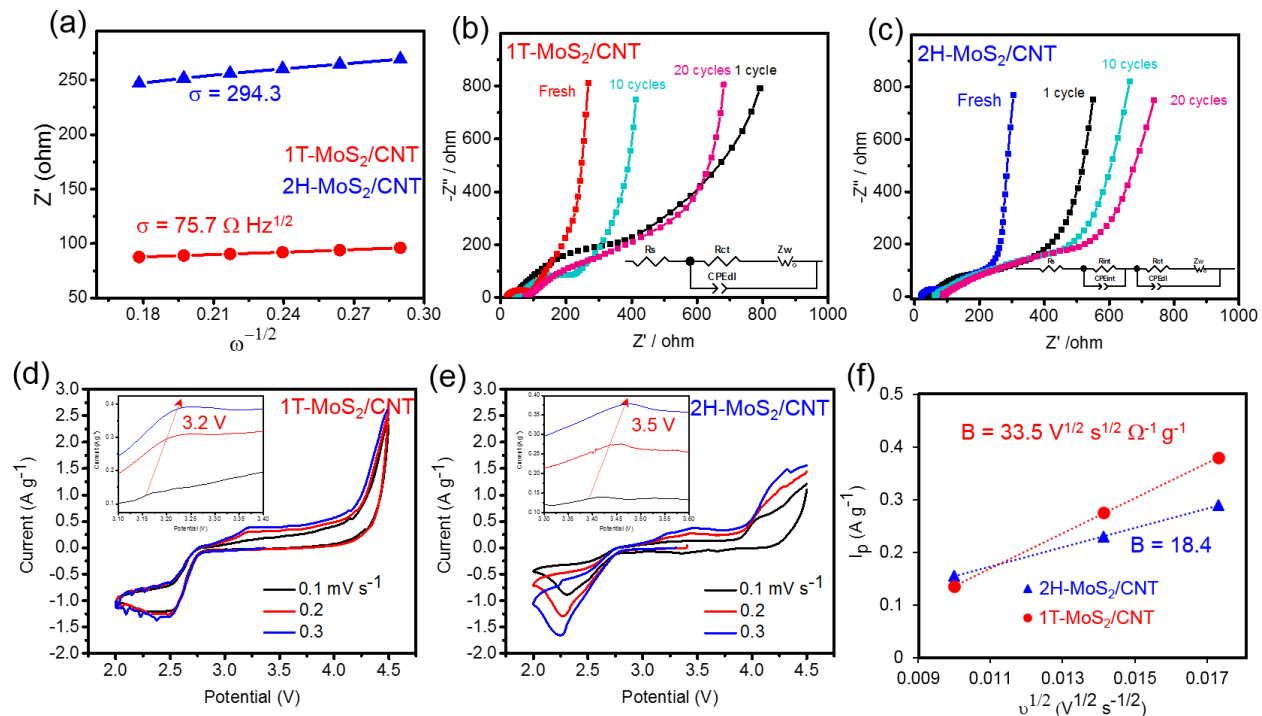


**Figure S6.**  $Z'$  versus minus square root of scanning frequency,  $\omega^{-1/2}$ , at a low frequency range of EIS spectra in Fig. 3g. EIS spectra of (b) 1T-MoS<sub>2</sub>/CNT and (c) 2H-MoS<sub>2</sub>/CNT electrodes obtained before and after one, 10, 20 and 40 full cycles (with the corresponding equivalent circuits shown in insets); CV curves of the (d) 1T-MoS<sub>2</sub>/CNT and (e) 2H-MoS<sub>2</sub>/CNT electrodes measured at the third and the following charge/discharge cycles at different scan rates; and (f) anodic peak current,  $I_p$ , versus square root of scan rate,  $v^{1/2}$ .

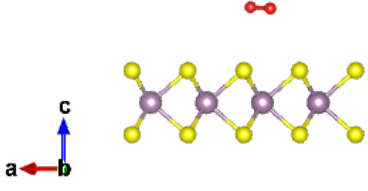
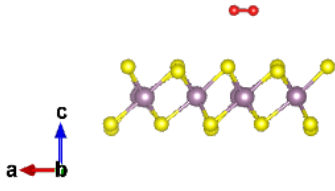
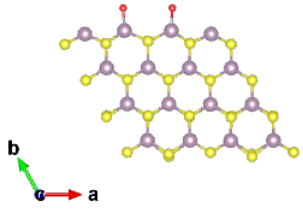
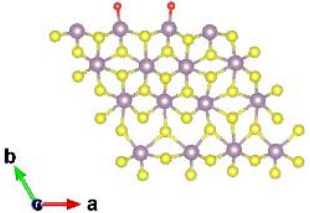
**Table S1.** Impedance parameters calculated using the equivalent circuits.

	$R_s / \Omega$	$R_{int} / \Omega$	$CPE_{int} / \mu F$	$R_{ct} / \Omega$	$CPE_{dl} / \mu F$	$Z_w / \Omega$
2H-MoS <sub>2</sub> /CNT	19.2	84.3	20.2	356.9	1142.5	480.1
1T-MoS <sub>2</sub> /CNT	18.7	—	—	83.6	21.5	56.4

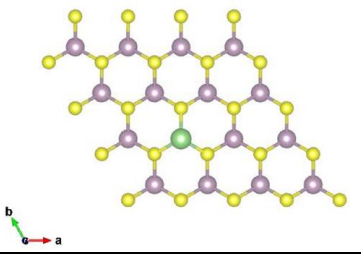
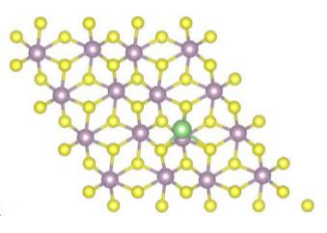
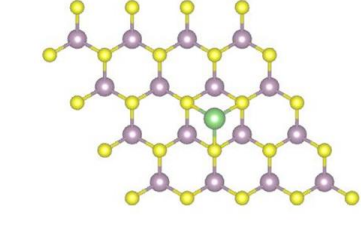
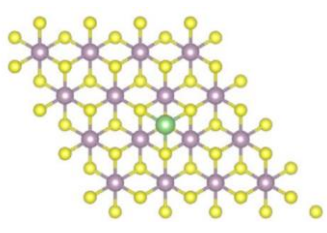
**Table S2.** Electrical conductivities, carrier concentrations and lithium diffusion coefficients of different electrodes.

	Electrical conductivity (S cm <sup>-1</sup> )	Carrier concentration (cm <sup>-3</sup> )	Lithium diffusion coefficient (cm <sup>2</sup> s <sup>-1</sup> )
1T-MoS <sub>2</sub> /CNT	54.6	-6.84 × 10 <sup>20</sup>	9.9 × 10 <sup>-10</sup>
2H-MoS <sub>2</sub> /CNT	10.7	+1.05 × 10 <sup>18</sup>	1.8 × 10 <sup>-11</sup>

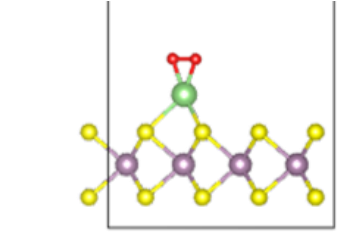
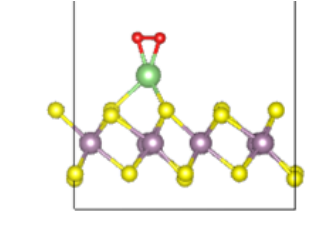
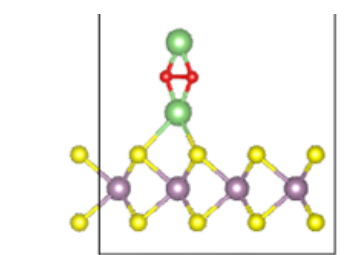
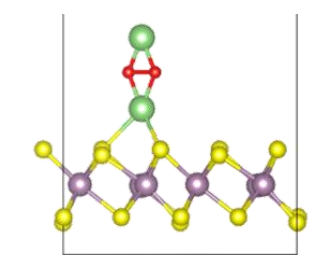
**Table S3.** Adsorption energies (eV) of O<sub>2</sub> molecules with different configurations on basal planes and Mo edges of 2H- and 1T-MoS<sub>2</sub>.

	2H-MoS <sub>2</sub>		1T-MoS <sub>2</sub>	
Basal plane	-0.095		-2.885	
Mo edge	-9.247		-8.622	

**Table S4.** Adsorption energies (eV) of Li on basal planes of 2H- and 1T-MoS<sub>2</sub> at different sites: Top of Mo (T) and hollow position (H).

	2H-MoS <sub>2</sub>		1T-MoS <sub>2</sub>	
Top of Mo (T)	-0.22		-4.68	
Hollow position (H)	-0.05		-4.55	

**Table S5.** Adsorption energies (eV) of Li<sub>x</sub>O<sub>y</sub> compounds on basal planes of 2H- and 1T-MoS<sub>2</sub>.

	2H-MoS <sub>2</sub>		1T-MoS <sub>2</sub>	
LiO <sub>2</sub>	-1.542		-5.169	
Li <sub>2</sub> O <sub>2</sub>	-3.144		-6.844	

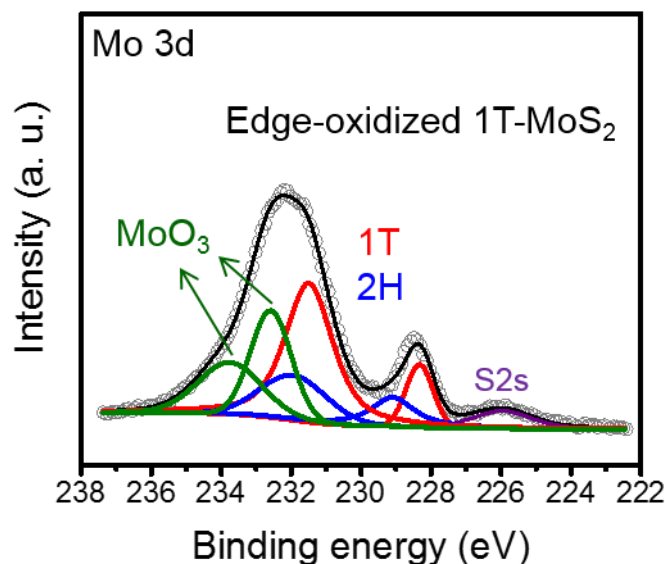


**Figure S7.** Deconvoluted Mo 3d XPS spectrum of edge-oxidized 1T-MoS<sub>2</sub>.

### SI References

- S1 D. Voiry, M. Salehi, R. Silva, T. Fujita, M. Chen, T. Asefa, V. B. Shenoy, G. Eda and M. Chhowalla, *Nano Lett.*, 2013, **13**, 6222–6227.
- S2 G. Eda, H. Yamaguchi, D. Voiry, T. Fujita, M. Chen and M. Chhowalla, *Nano Lett.*, 2011, **11**, 5111–5116.
- S3 H. Wang, Z. Sofer, J. G. S. Moo and M. Pumera, *Chem. Commun.*, 2015, **51**, 9899–9902.
- S4 M. Wu, J. Zhan, K. Wu, Z. Li, L. Wang, B. Geng, L. Wang and D. Pan, *J. Mater. Chem. A*, 2017, **5**, 14061–14069.
- S5 I. Kruusenberg, N. Alexeyeva, K. Tammeveski, J. Kozlova, L. Matisen, V. Sammelselg, J. Solla-Gullon and J. M. Feliu, *Carbon*, 2011, **49**, 4031–4039.
- S6 Z. Sadighi, J. Huang, L. Qin, S. Yao, J. Cui and J.-K. Kim, *J. Power Sources*, 2017, **365**, 134–147.
- S7 Z. Sadighi, J. Liu, F. Ciucci and J.-K. Kim, *Nanoscale*, 2018.
- S8 C. Du, H. Huang, X. Feng, S. Wu and W. Song, *J. Mater. Chem. A*, 2015, **3**, 7616–7622.
- S9 I. S. Amiin, Z. Pu, X. Liu, K. A. Owusu, H. G. R. Monestel, F. O. Boakye, H. Zhang and S. Mu, *Adv. Funct. Mater.*
- S10 X. Shang, W.-H. Hu, X. Li, B. Dong, Y.-R. Liu, G.-Q. Han, Y.-M. Chai and C.-G. Liu,

- Electrochim. Acta*, 2017, **224**, 25–31.
- S11 Z.-Q. Liu, H. Cheng, N. Li, T. Y. Ma and Y.-Z. Su, *Adv. Mater.*, 2016, **28**, 3777–3784.
- S12 S. Yao, J. Cui, Z. Lu, Z.-L. Xu, L. Qin, J. Huang, Z. Sadighi, F. Ciucci and J.-K. Kim, *Adv. Energy Mater.*
- S13 J. Cui, S. Yao, Z. Lu, J.-Q. Huang, W. G. Chong, F. Ciucci and J.-K. Kim, *Adv. Energy Mater.*
- S14 G. Kresse, *Phys. Rev. B*, 1996, **54**, 11169.
- S15 P. E. Blöchl, *Phys. Rev. B*, 1994, **50**, 17953.
- S16 J. P. Perdew, K. Burke and M. Ernzerhof, *Phys. Rev. Lett.*, 1996, **77**, 3865.
- S17 S. Grimme, J. Antony, S. Ehrlich and H. Krieg, *J. Chem. Phys.*, 2010, **132**, 154104.
- S18 M. Mortazavi, C. Wang, J. Deng, V. B. Shenoy and N. V Medhekar, *J. Power Sources*, 2014, **268**, 279–286.
- S19 X. Li, Z. Li, X. Yang, L. Jia, Y. Q. Fu, B. Chi, J. Pu and J. Li, *J. Mater. Chem. A*, 2017, **5**, 3320–3329.
- S20 H.-G. Jung, J. Hassoun, J.-B. Park, Y.-K. Sun and B. Scrosati, *Nat. Chem.*, 2012, **4**, 579–585.
- S21 J. Cui, Z.-L. Xu, S. Yao, J. Huang, J.-Q. Huang, S. Abouali, M. A. Garakani, X. Ning and J.-K. Kim, *J. Mater. Chem. A*, 2016, **4**, 10964–10973.